Comparison of saturator designs for delivery of low-volatility liquid precursors

James E. Maslar,[*,1] William A. Kimes,[1] Vladimir B. Khromchenko,[1] Brent A. Sperling,[2] and Ravindra K. Kanjolia[3]

[1]National Institute of Standards and Technology, 100 Bureau Drive, Gaithersburg, MD 20899

[2]EMD Electronics, Tamaqua, PA 18252

[3]EMD Electronics, Haverhill, MA 01832

[*]Corresponding author: E-mail: jmaslar@nist.gov

ABSTRACT

Numerous low-volatility precursors are utilized in chemical vapor deposition and atomic layer deposition processes. Such precursors are often delivered from one of two common saturator designs: a bubbler or a flow over vessel. Previous reports concerning precursor delivery from such vessels have focused primarily on continuous delivery of moderate to high volatility liquids and solids. Few reports have focused on cyclical delivery of low volatility precursors at reduced pressures. This lack of knowledge concerning such processes can be a hindrance to efficient selection of deposition conditions and vessel design. The objective of this investigation was to compare the performance of these two saturator designs for pulsed injection at reduced pressures using the low volatility liquid precursor μ^2-η^2-(^{t}Bu-acetylene) dicobalthexacarbonyl (CCTBA). The basis of this comparison was the measurement of CCTBA mass carryover per injection as a function of injection number, injection time, carrier gas flow rate, system pressure, and vessel idle time. The mass carryover was determined from absorbance measurements performed using a non-dispersive infrared gas analyzer. The measured mass carryover for both vessels was compared to the theoretical mass carryover determined using a simple analytical model based upon the "bubbler equation". In the case of the bubbler, this model described the vessel performance well with knowledge of the precursor vapor pressure and vessel head space pressure. In the case of the flow over vessel, this model described the overall vessel performance poorly unless an additional vessel efficiency factor was included, a factor that is difficult to predict *a priori*. Furthermore, the efficiency factor was not necessarily constant for a series of injections: the efficiency factor tended to decrease from the first injection until a stable value was achieved, a value that depended on the process conditions. This limitation of the model was attributed to the specific flow dynamics associated with the flow over vessel design. Computational fluid dynamics simulations were able

to reproduce the mass carryover of the flow over vessel, after estimating the CCTBA-carrier gas binary diffusion coefficient. These simulations also showed that a larger binary diffusion coefficient and a higher vapor pressure both led to an increase in mass carryover but vessel efficiency could not equal that of the bubbler. While these results were obtained with CCTBA, the general relationships between mass carryover and the various process parameters in these saturators are expected to be similar for other low-volatility precursors.

1. Introduction

Numerous low-volatility precursors are utilized in chemical vapor deposition (CVD) and atomic layer deposition (ALD) processes. Such precursors are often delivered from the precursor vessel to the deposition surface by evaporating (subliming) a liquid (solid) precursor to generate a vapor which is entrained in a carrier gas. Ideally, the carrier gas is saturated in the vessel head space with the precursor vapor at the precursor vapor pressure. Most previous reports describing saturator design and performance were focused on continuous delivery of moderate to high volatility precursors for CVD or organometallic vapor phase epitaxy (OMVPE) processes.[1-27] When describing liquid precursor delivery, previous reports have naturally focused on bubblers.[2, 4, 6-13, 25-27] (In this work, a “bubbler” refers to a vessel configured with a dip tube on the gas inlet port that extends nearly to the bottom of the vessel.) However, even when describing solid precursor delivery, the majority of previous reports focused on saturator designs in which the carrier gas was directed through the precursor bed. Such designs include inverted or reverse bubbler-type vessels and sometimes incorporate restricted flow paths with multiple trays or chambers.[1, 3-6, 10, 13-24] While such designs have been shown to provide excellent performance (at least under some conditions), these designs can be more costly to manufacture and clean. Hence, simpler flow over vessels are often utilized for precursor delivery. (In this work, a “flow over vessel” refers to a vessel through which carrier gas flows but which has no dip tube: the gas inlet and outlet ports open directly into the vessel head space.)

Previous precursor delivery studies have helped to identify process conditions and vessel design characteristics that are desirable for continuous delivery of moderate to high volatility precursors for CVD or OMVPE processes, often at elevated pressures. However, the process conditions and vessel characteristics that are desirable for pulsed delivery of low volatility precursors at reduced pressures have not been widely identified. There are a few reports describing precursor delivery under such conditions, including a liquid from a bubbler[28] and a solid from a flow over vessel.[29, 30] However, it is difficult to compare definitively the performance of a bubbler and flow over vessel from these reports because the precursors and flow conditions were different. It is well known that a number of factors can lead to non-reproducible delivery of solid precursors and that these factors can be related both to the physicochemical properties of the precursor and the flow characteristics of the respective precursor vessel.[1, 3-5, 10, 15, 16, 18, 19, 21, 23, 24, 30-32] Therefore, it is sometimes difficult to differentiate between the impact on delivery of vessel flow characteristics and precursor properties. Hence, a more straight-forward comparison of vessel designs for precursor delivery would involve the same precursor.

The objective of this investigation was to compare directly the performance of a bubbler and a flow over vessel for delivery of low-volatility precursors during reduced-pressure, cyclical deposition processes, e.g., pulsed CVD and ALD processes. The same liquid precursor, μ^2-η^2-(^{t}Bu-acetylene) dicobalthexacarbonyl (CCTBA), was utilized in both vessels. A liquid was examined to avoid any additional complications that can be associated with the use of solids, thereby permitting a more straight-forward comparison of the vessel performance. The basis of this comparison was the measurement of CCTBA mass carryover per injection as a function of injection number, duration of precursor injection (t_{inj}), carrier gas flow rate, system pressure, and duration of the vessel idle between injections (t_{idle}). Mass values were obtained from direct absorbance measurements performed using a non-dispersive infrared (NDIR) gas analyzer. The measured mass carryover for both vessels was compared to the theoretical mass carryover determined from a model based upon the "bubbler equation".[2, 7-11, 33] The mass carryover from the flow over vessel was also compared to that obtained from computational fluid dynamics (CFD) simulations. The focus of this investigation was on the following delivery conditions: $t_{inj} \leq 2$ s, $t_{idle} \leq 8$ s or $t_{idle} \geq 180$ s, vessel head space pressures between 1.2 kPa and 7.8 kPa, and carrier gas flow rates ranging from 0.25 L/min to 0.75 L/min. The results of this study should help elucidate the impact of process conditions and vessel design on precursor delivery for two common saturator designs operating under process conditions that are not widely reported upon.

2. Experimental procedure

2.1. Materials

A stainless steel bubbler and flow over vessel were compared. Each vessel had nominally the same ≈ 1.5 L volume and specific dimensions, as described elsewhere.[30] Approximately 200 g of microelectronics-grade CCTBA (EMD Electronics[†]) was supplied in each vessel (the CCTBA was used as received). Ultra-high-purity grade argon was used as the carrier gas and was further purified with a point-of-use purifier.

2.2 Flow system

The design and operation of the flow system have been described previously[34, 35] and will only be described briefly. A schematic of the flow system used for each vessel is shown in Fig. 1. The carrier gas flow rate was controlled with a mass flow controller (MFC) and the system pressure was measured using one capacitance diaphragm gauge upstream of the precursor vessel (CDG1) and one downstream (CDG2). The total pressure at CDG1 and CDG2 are designated by P^{CDG1} and P^{CDG2}, respectively. Optical access to the gas flow was achieved with one of two optical flow cells

[†] Certain commercial equipment, instruments, and materials are identified in this publication to adequately specify the experimental procedure. Such identification in no way implies approval, recommendation, or endorsement by the National Institute of Standards and Technology, nor does it imply that the equipment, instruments, or materials identified are necessarily the best available for the purpose.

(FC1 and FC2) located downstream of the precursor vessel. The conductance of the flow system was adjusted using a manual throttle valve (TV). Five valves were used to control gas distribution: three pneumatic valves (PV_{in}, PV_{by}, and PV_{out}) to control gas switching during a run and two manual valves (MV_{in} and MV_{out}) to isolate the vessel when not in use (the manual valves were open for all measurements). PV_{in} and MV_{in} and PV_{out} and MV_{out} were located on the inlet and outlet lines of the vessel, respectively. PV_{by} was located on the line that bypasses the vessel. For the bubbler [see Fig. 1(a)], PV_{in}, PV_{by}, and PV_{out} were 2-port valves while MV_{in} and MV_{out} were 3-port valves. The 3-port valves on the bubbler were configured in a "T" in which one side of the arm of the "T" was valved and flow was unimpeded from the stem of the "T" through the non-valved side of the arm. For the flow over vessel [see Fig. 1(b)], PV_{by}, MV_{in}, and MV_{out} were 2-port valves while PV_{in} and PV_{out} were 3-port valves. The 3-port valves on the flow over vessel were configured in a "T" in which the stem of the "T" was valved and flow was unimpeded through the arm of the "T". Gas flow was initiated in the vessel-idle/line-purge configuration (no flow through the vessel) by opening PV_{by} (while PV_{in} and PV_{out} were closed), setting the MFC to the desired flow rate, and adjusting TV to obtain the desired pressure at CDG2. In the injection configuration, carrier gas was directed through the vessel by opening PV_{in} and PV_{out} (while PV_{by} was closed). The argon flow rates employed in this work were 0.25 L/min, 0.50 L/min, and 0.75 L/min at standard temperature and pressure (STP), defined as 0 °C and 101.33 kPa, respectively. In subsequent discussions, flow rates are referenced to STP. The TV was set to provide either 1.3 kPa or 4.7 kPa at CDG2 for a 0.50 L/min flow rate and not adjusted subsequently. The flow conditions are summarized in Table I. All surfaces from CDG1 to TV were heated. The sublimator, FC1, and FC2 were encased in aluminum jackets which were heated with strip and cartridge heaters, respectively. Lines and valves were wrapped and heated with heating tapes (the valves were mounted on aluminum blocks to facilitate heat distribution). All heated components were insulated with high-temperature silicone foam. The temperature setpoint for the vessel, the valves and inlet line, and the rest of the flow system were 50 °C, 55 °C, and 63 °C, respectively.

Table I. The TV designations and the associated argon flow rate and total pressure at CDG2 used for setting the conductance and the corresponding conditions during measurements.

	Conditions for setting conductance		Conditions for measurements	
	Ar flow rate	P^{CDG2}	Ar flow rate	P^{CDG2}
Designation	**(**L/min**)**	(kPa)	**(**L/min**)**	(kPa)
TV-1	0.50	1.3	0.25	0.7 to 1.0
			0.50	1.1 to 1.6
			0.75	1.6 to 2.1
TV-2	0.50	4.7	0.25	2.6 to 2.9
			0.50	4.4 to 4.9
			0.75	6.0 to 6.6

2.3 NDIR gas analyzer

The NDIR gas analyzer has been described elsewhere[35] and will only be described briefly. Analyzer operation was based on a direct absorption measurement of CCTBA in the C≡O stretching mode spectral region. Analyzer design included a broadband infrared source, a 4.95 μm center-wavelength bandpass filter, and a cryogenically-cooled indium antimonide detector. Measurements were performed in a single pass through FC1 (the optical axis was perpendicular to the direction of gas flow). The CCTBA volumetric flow rate at STP ($F_{\mathrm{CCTBA}}^{\mathrm{STP}}$) was calculated using the bubbler equation[2, 7-11, 33]

$$F_{\mathrm{CCTBA}}^{\mathrm{STP}} = F_{\mathrm{Ar}}^{\mathrm{STP}} \frac{P_{\mathrm{CCTBA}}^{\mathrm{FC1}}}{\left(P_{\mathrm{ttl}}^{\mathrm{FC1}} - P_{\mathrm{CCTBA}}^{\mathrm{FC1}}\right)} \tag{1}$$

where $F_{\mathrm{Ar}}^{\mathrm{STP}}$ is the carrier gas volumetric flow rate (STP), $P_{\mathrm{CCTBA}}^{\mathrm{FC1}}$ is the CCTBA partial pressure at FC1, and $P_{\mathrm{ttl}}^{\mathrm{FC1}}$ is the total pressure at FC1. $P_{\mathrm{CCTBA}}^{\mathrm{FC1}}$ was determined from the absorbance measurements[35] and $P_{\mathrm{ttl}}^{\mathrm{FC1}}$ was obtained from P^{CDG2} by calculating the pressure drop that exists between CDG2 and FC1 using the Hagen-Poiseuille equation.[34, 35]

2.4. Calculating CCTBA Mass Delivered

The calculated CCTBA mass delivered per injection ($m_{\mathrm{inj}}^{\mathrm{c}}$) is described by [33, 36]

$$m_{\mathrm{inj}}^{\mathrm{c}} = F_{\mathrm{CCTBA}}^{\mathrm{STP}} \left(\frac{P^{\mathrm{STP}} M}{R T^{\mathrm{STP}}}\right) t_{\mathrm{inj}} = F_{\mathrm{Ar}}^{\mathrm{STP}} \frac{P_{\mathrm{CCTBA}}^{\mathrm{HS}}}{P_{\mathrm{Ar}}^{\mathrm{HS}}} \left(\frac{P^{\mathrm{STP}} M}{R T^{\mathrm{STP}}}\right) t_{\mathrm{inj}} = F_{\mathrm{Ar}}^{\mathrm{STP}} \frac{\bar{\eta}_{\mathrm{S}} P_{\mathrm{CCTBA}}^{\mathrm{VP}}}{\left(P_{\mathrm{ttl}}^{\mathrm{HS}} - P_{\mathrm{CCTBA}}^{\mathrm{HS}}\right)} \left(\frac{P^{\mathrm{STP}} M}{R T^{\mathrm{STP}}}\right) t_{\mathrm{inj}} \tag{2}$$

where P^{STP} is the standard pressure, M is the precursor molar mass, R is the gas constant, T^{STP} is the absolute standard temperature, $P_{\mathrm{CCTBA}}^{\mathrm{HS}}$, $P_{\mathrm{Ar}}^{\mathrm{HS}}$, and $P_{\mathrm{ttl}}^{\mathrm{HS}}$ are the precursor partial pressure, carrier gas partial pressure, and total system pressure, respectively, in the vessel head space ($P_{\mathrm{ttl}}^{\mathrm{HS}}$ = $P_{\mathrm{CCTBA}}^{\mathrm{HS}}$ + $P_{\mathrm{Ar}}^{\mathrm{HS}}$), $\bar{\eta}_{\mathrm{S}}$ is the average source efficiency factor, and $P_{\mathrm{CCTBA}}^{\mathrm{VP}}$ is the CCTBA vapor pressure. The term $\bar{\eta}_{\mathrm{S}}$ represents the degree to which the condition $P_{\mathrm{CCTBA}}^{\mathrm{HS}} \approx P_{\mathrm{CCTBA}}^{\mathrm{VP}}$ is realized and is defined as[36]

$$\bar{\eta}_{\mathrm{S}} = \frac{m_{\mathrm{inj}}^{\mathrm{m}}}{m_{\mathrm{inj}}^{1}} = \frac{1}{t_{\mathrm{inj}}} \int_{0}^{t_{\mathrm{inj}}} \eta_{\mathrm{S}}(t)\, dt = \frac{1}{t_{\mathrm{inj}}} \int_{0}^{t_{\mathrm{inj}}} \frac{P_{\mathrm{CCTBA}}^{\mathrm{HS}}(t)}{P_{\mathrm{CCTBA}}^{\mathrm{VP}}} dt \tag{3}$$

where $m_{\mathrm{inj}}^{\mathrm{m}}$ is the measured CCTBA mass delivered per injection, and m_{inj}^{1} is the mass per injection from a perfectly efficient vessel as calculated using Eq. (2) with $\bar{\eta}_{\mathrm{S}} = 1$, $\eta_{\mathrm{S}}(t)$ represents the time-dependent instantaneous source efficiency, and $P_{\mathrm{CCTBA}}^{\mathrm{HS}}(t)$ represents the time-dependent $P_{\mathrm{CCTBA}}^{\mathrm{HS}}$.

The total pressure in the head space was assumed to be the average of P^{CDG1} and the pressure at a location downstream of the last outlet valve. This location was ≈18 cm from $\mathrm{MV_{out}}$ and ≈6 cm from $\mathrm{PV_{out}}$ for the bubbler and flow over vessel, respectively (≈114.5 cm from CDG2 in both cases). The pressure at the respective outlet location was calculated by taking into account the pressure drop between this location and CDG2 using the Hagen-Poiseuille equation. The pressure increase from CDG2 to this location was ≤ 10 % and ≤ 1 % for TV-1 and TV-2, respectively. When tabulating the $P_{\mathrm{ttl}}^{\mathrm{HS}}$ values, an average value was calculated over a time interval determined from the inflection points of the derivative of P^{CDG2}, with 0.1 s and 0.175 s added to the start and subtracted from the end of the interval, respectively, to reduce the effect on this estimation of pressure transients during valve switching. In the case of the bubbler, the hydrostatic pressure, P_{hydro}, was subtracted from P^{CDG1} prior to calculating the average value[33]

$$P_{\mathrm{hydro}} = \rho_{\mathrm{CCTBA}}\, g l \tag{4}$$

where ρ_{CCTBA} is the CCTBA density (assumed to be 1440 kg/m^3), g is the acceleration of gravity, and l is the length of the dip tube below the CCTBA level (there is a 2 mm distance between the bottom of the dip tube and bottom of the vessel). Depending on the mass in the bubbler, the estimated P_{hydro} value ranged from 127 Pa to 79 Pa for 200 g (the mass as received) to 139 g (the mass remaining after the measurements described here), respectively. For simplicity, the average P_{hydro} = 103 Pa was used for all estimations. This method of estimating $P_{\mathrm{ttl}}^{\mathrm{HS}}$ assumes an equal pressure drop across each of the four valves during injection. This has been shown to be a reasonable assumption for at least one empty bubbler with $P^{\mathrm{CDG2}} \approx 5.2$ kPa.[34] However, valve conductance can vary from valve to valve so the relevance of this previous report is uncertain.

The value of $P_{\mathrm{CCTBA}}^{\mathrm{VP}}$ is described by the Antoine equation:

$$\log_{10} P_{\mathrm{CCTBA}}^{\mathrm{VP}} = A_{\mathrm{A}} - B_{\mathrm{A}}/T \tag{5}$$

where T is the absolute temperature and A_{A} and B_{A} are constants equal to 11.39 and 3209.3, respectively.[28] From this expression, $P_{\mathrm{CCTBA}}^{\mathrm{VP}}$ = 28.8 Pa at 50 °C.

2.5. Computational fluid dynamics simulations

CFD simulations of delivery from the flow over vessel were performed using COMSOL Multiphysics version 6.0, as described previously for a low volatility solid in an identical vessel design as utilized in this study.[30] To simplify these simulations, it was assumed that the gas properties were those of argon (CCTBA was dilute), that the pressure was constant (given by $P_{\mathrm{ttl}}^{\mathrm{HS}}$), that the only source of CCTBA was vapor above the liquid at the bottom of the vessel, and the CCTBA partial pressure was equal to the vapor pressure. The properties of argon were obtained from REFPROP.[37] The binary diffusion coefficient (D_{AB}) was calculated from[38]

$$D_{\mathrm{AB}} = \frac{3}{16} \frac{\left(4\pi k_{\mathrm{B}} T / m_{\mathrm{AB}}\right)^{1/2}}{n\pi\sigma_{\mathrm{AB}}^{2}\Omega_{D}} f_{D} = d_{0} T^{3/2} / P_{\mathrm{ttl}}^{\mathrm{HS}} \tag{6}$$

where k_{B} is the Boltzmann constant, $m_{\mathrm{AB}} = 2\left[\left(1/m_{\mathrm{A}}\right) + \left(1/m_{\mathrm{B}}\right)\right]^{-1}$ where m_{A} and m_{B} are the molecular mass of molecule A and B, n is the number density of molecules, σ_{AB} is the characteristic length, Ω_{D} is the collision integral, and f_{D} is a correction term. To simulate $m_{\mathrm{inj}}^{\mathrm{m}}$, a value of $d_0 = 3.5 \times 10^{-5}$ kg·m·s^{-3}·K$^{-3/2}$ ($m_{\mathrm{inj}}^{\mathrm{CFD}}$) at 50 °C was selected. Using this d_0 value, the mass difference between $m_{\mathrm{inj}}^{\mathrm{m}}$ and $m_{\mathrm{inj}}^{\mathrm{CFD}}$ for fifteen injections with $F_{\mathrm{Ar}}^{\mathrm{STP}}$ = 0.75 L/min, t_{inj} = 2 s, t_{idle} = 8 s, and in the TV-2 flow configuration was < 2 % for each injection number four through fifteen (see Fig. 6 and associated discussion).

3. Results and discussion

Figure 2 shows the $m_{\mathrm{inj}}^{\mathrm{m}}$ values as a function of injection number for the bubbler and flow over vessels with $F_{\mathrm{Ar}}^{\mathrm{STP}}$ = 0.50 L/min, t_{inj} = 2 s, t_{idle} = 8 s, and in the TV-2 flow configuration. Also shown are dashed and dot-dashed lines that represent the $m_{\mathrm{inj}}^{\mathrm{c}}$ values for the bubbler and flow over vessel, respectively, calculated with the $\bar{\eta}_{\mathrm{S}}$ values indicated on each line. There is good agreement between $m_{\mathrm{inj}}^{\mathrm{m}}$ and m_{inj}^{1} as expected.[28] In the case of the bubbler, the mass carryover decreases slightly from the first injection to a stable mass carryover after about three injections. The small decrease in mass for the first one to two injections is attributed to the time it takes for the pressure in the system to stabilize from pulse to pulse (see Fig. 3 and associated discussion). Once a stable mass carryover is observed after the first one to two injections, the m_{inj}^{1} values are about 3 % lower than the $m_{\mathrm{inj}}^{\mathrm{m}}$ values, a difference which is attributed to the simplistic method used to estimate $P_{\mathrm{ttl}}^{\mathrm{HS}}$ (see Sec. 2.4). In the case of the flow over vessel, there is relatively poor agreement between $m_{\mathrm{inj}}^{\mathrm{m}}$ and m_{inj}^{1} as has been observed previously for a solid in such a vessel design.[29] The $\bar{\eta}_{\mathrm{S}}$ values range from about 0.77 for the first injection to about 0.44 once a stable mass carryover has been achieved after about twenty to thirty injections. As noted previously, the method used to estimate $P_{\mathrm{ttl}}^{\mathrm{HS}}$ results in an underestimation of m_{inj}^{1} in the case of the bubbler. Presumably, this also is the case for the flow over vessel. Hence, the calculated $\bar{\eta}_{\mathrm{S}}$ values are likely overestimated by an amount corresponding to the degree of underestimation of m_{inj}^{1}. The observed decrease of mass carryover with injection number until a stable mass carryover is achieved is characteristic of a flow over vessel. This behavior is explained as follows. Prior to the first injection, the vessel was subjected to a >300 s idle during which CCTBA vapor diffused into the vessel head space until $P_{\mathrm{CCTBA}}^{\mathrm{HS}}$ = $P_{\mathrm{CCTBA}}^{\mathrm{VP}}$, the maximum CCTBA partial pressure achievable. The $m_{\mathrm{inj}}^{\mathrm{m}}$ value decreases from that of a preceding injection when the amount of CCTBA removed during an injection is greater than the sum of the amount of CCTBA diffusing into the head space during the preceding idle (an 8 s idle is insufficient to result in $P_{\mathrm{CCTBA}}^{\mathrm{HS}} = P_{\mathrm{CCTBA}}^{\mathrm{VP}}$) plus the amount being entrained into the flowing carrier gas from the precursor reservoir. A stable mass carryover is achieved when the amount of CCTBA removed during an injection equals the sum of the amount diffusing into the headspace plus the amount being entrained. As described in the case of the bubbler, pressure stabilization effects led to the first one to two injections exhibiting a higher $m_{\mathrm{inj}}^{\mathrm{m}}$ than subsequent injections. In the case of the flow over vessel, similar effects are present, but it is difficult to differentiate the effects on $m_{\mathrm{inj}}^{\mathrm{m}}$ of pressure stabilization and gas flow dynamics (see Fig. 3 and associated discussion). However, the pressure stabilization process presumably results in a less sharp decrease from the first injection than would have been observed in the absence of this effect. Because of these flow characteristics, Eq. (2) with a constant $\bar{\eta}_{\mathrm{S}}$ value does not describe the flow over vessel performance for all injections. However, this equation with a constant $\bar{\eta}_{\mathrm{S}}$ value can adequately describe the performance once a stable mass carryover is achieved, as illustrated by the dot-dashed line labeled with $\bar{\eta}_{\mathrm{S}}$ = 0.44 (a value obtained from the average $\bar{\eta}_{\mathrm{S}}$ value for injections 51 to 100).

Figure 3 shows the time-dependent (a) $P_{\mathrm{CCTBA}}^{\mathrm{FC}}$ and (b) P^{CDG2} values for the first five injections from the bubbler and (c) $P_{\mathrm{CCTBA}}^{\mathrm{FC}}$ and (d) P^{CDG2} for the first ten injections from the flow over vessel, all with $F_{\mathrm{Ar}}^{\mathrm{STP}}$ = 0.50°L/min, t_{inj} = 2 s, t_{idle} = 8 s, and in the TV-2 flow configuration (the same conditions as for Fig. 2). In the case of the bubbler, the time-dependent $P^{\mathrm{FC}}_{\mathrm{CCTBA}}$ profile is rectangular and does not vary significantly with injection number while P^{CDG2} increases slightly over the first two to three injections. These trends are consistent with those observed in Fig. 2: the $m^{\mathrm{m}}_{\mathrm{inj}}$ value is relatively stable except for the first two injections during which the system pressure is increasing, leading to a decrease in $m^{\mathrm{m}}_{\mathrm{inj}}$ at constant $P^{\mathrm{HS}}_{\mathrm{CCTBA}}$ as expected from Eq. (2). In the case of the flow over vessel, the time-dependent $P^{\mathrm{FC}}_{\mathrm{CCTBA}}$ profile is also rectangular but decreases with injection number for more than the first ten injections. In addition, the time-dependence of $P^{\mathrm{FC}}_{\mathrm{CCTBA}}$ is different for first injection compared to the other four, the time-dependence of which are similar. The P^{CDG2} value increases over only the first four injections. These results are consistent with the explanation of the trends observed in Fig. 2: pressure stabilization may impact the $m^{\mathrm{m}}_{\mathrm{inj}}$ value for the first one to four injections but the $m^{\mathrm{m}}_{\mathrm{inj}}$ value continues to decrease beyond four injections due to the gas dynamics in the flow over vessel, driven by the continued decrease of CCTBA partial pressure. The difference in $P^{\mathrm{FC}}_{\mathrm{CCTBA}}$ for the first injection compared to that of subsequent injections is attributed to pressure stabilization in the valve manifold after a long idle. Presumably, this effect is not observed for the bubbler because the volume associated with the bubbler valve manifold is smaller than that of the flow over vessel (see Fig. 1).

The dependence of the mass carryover on t_{inj} is depicted in Fig. 4 which shows the $m^{\mathrm{m}}_{\mathrm{inj}}$ value as a function of t_{inj} for the TV-1 and TV-2 flow configurations with the bubbler for $F^{\mathrm{STP}}_{\mathrm{Ar}}$ = (a) 0.25 L/min, (b) 0.50 L/min, and (c) 0.75 L/min and the flow over vessel for $F^{\mathrm{STP}}_{\mathrm{Ar}}$ = (d) 0.25 L/min, (e) 0.50 L/min, and (f) 0.75 L/min. For each injection, $t_{\mathrm{idle}} = 4 \times t_{\mathrm{inj}}$. The larger $m^{\mathrm{m}}_{\mathrm{inj}}$ values at the top of the vertical stack correspond to earlier injections while the grouping of symbols at the smaller $m_{\mathrm{inj}}^{\mathrm{m}}$ values corresponds to a state of stable mass carryover. The dashed and dot-dashed lines represent the $m_{\mathrm{inj}}^{\mathrm{c}}$ values for TV-1 and TV-2, respectively, calculated with the $\bar{\eta}_{\mathrm{S}}$ values indicated on each line. In the case of the bubbler [Fig. 4(a) to 4(c)], the $m_{\mathrm{inj}}^{\mathrm{m}}$ value increases with increasing t_{inj} and $F_{\mathrm{Ar}}^{\mathrm{STP}}$ and decreasing P^{CDG2}. All of these relationships are described well by Eq. (2) with $\bar{\eta}_{\mathrm{S}}$ equal to unity. As was the case for the data shown in Fig. 2, the m_{inj}^{1} values are slightly lower than the $m_{\mathrm{inj}}^{\mathrm{m}}$ values for some conditions, particularly at lower P^{CDG2}. This underestimation again is attributed to the simplistic method used to estimate $P_{\mathrm{ttl}}^{\mathrm{HS}}$. The difference between the $m_{\mathrm{inj}}^{\mathrm{m}}$ and m_{inj}^{1} values is greater in the TV-1 configuration compared to the TV-2 configuration because the pressure drop across the valve manifold is greater in the former, resulting in a poorer estimate of $P_{\mathrm{ttl}}^{\mathrm{HS}}$. In the case of the flow over vessel [Fig. 4(d) to 4(f)], for the first injection the $m_{\mathrm{inj}}^{\mathrm{m}}$ value increases with increasing t_{inj} and $F_{\mathrm{Ar}}^{\mathrm{STP}}$ and decreasing P^{CDG2}. Once a stable mass carryover is achieved, the $m_{\mathrm{inj}}^{\mathrm{m}}$ value increases with increasing t_{inj}, however, the $m_{\mathrm{inj}}^{\mathrm{m}}$ value increases relatively little with decreasing P^{CDG2} (in the range investigated here) and decreases slightly with increasing $F_{\mathrm{Ar}}^{\mathrm{STP}}$ (in contrast to the behavior observed with the bubbler). The relatively weak dependence of $m_{\mathrm{inj}}^{\mathrm{m}}$ on pressure and the inverse dependence on flow rate are contrary to the dependence expected based on Eq. (2). These characteristics are attributed to the flow dynamics of the flow over vessel. The $m_{\mathrm{inj}}^{\mathrm{m}}$ values at a stable mass carryover are reasonably well described by Eq. (2) with constant $\bar{\eta}_{\mathrm{S}}$ obtained from the average $\bar{\eta}_{\mathrm{S}}$ value for injections 51 to 100 of the respective run (as was illustrated in Fig. 2). For the flow over vessel, the respective $\bar{\eta}_{\mathrm{S}}$ value decreases with decreasing P^{CDG2} and increasing $F_{\mathrm{Ar}}^{\mathrm{STP}}$.

The dependence of the mass carryover on t_{idle} is illustrated in Fig. 5 which shows the $m_{\text{inj}}^{\text{m}}$ value as a function of t_{idle} for t_{inj} = 0.5 s in the TV-1 and TV-2 flow configurations with the bubbler for $F_{\text{Ar}}^{\text{STP}}$ = (a) 0.25 L/min, (b) 0.50 L/min, and (c) 0.75 L/min and the flow over vessel for $F_{\text{Ar}}^{\text{STP}}$ = (d) 0.25 L/min, (e) 0.50 L/min, and (f) 0.75 L/min. The dashed and dot-dashed lines represent the $m_{\text{inj}}^{\text{c}}$ values for TV-1 and TV-2, respectively, calculated with the indicated $\bar{\eta}_{\text{S}}$ values. In the case of the bubbler [Fig. 5(a) to 5(c)], the mass delivered is independent of t_{idle}, indicating that the head space is saturated at the precursor vapor pressure for all conditions. As was the case previously, Eq. (2) with $\bar{\eta}_{\text{S}}$ equal to unity describes the bubbler performance, although the $P_{\text{ttl}}^{\text{HS}}$ estimation method again results in an underestimation of mass carryover for some conditions. In the case of the flow over vessel [Fig. 5(d) to 5(f)], the $m_{\text{inj}}^{\text{m}}$ values for each first injection are approximately independent of t_{idle}, while the $m_{\text{inj}}^{\text{m}}$ values under stable mass carryover conditions increase with increasing t_{idle}. The underlying process responsible for this behavior is diffusion of CCTBA into the vessel head space during idle/purge. The vessel was idled for longer than 300 s between each run, resulting in $P_{\text{CCTBA}}^{\text{HS}} \approx P_{\text{CCTBA}}^{\text{VP}}$. Hence, $m_{\text{inj}}^{\text{m}}$ was approximately the same for the first injection of each run since t_{inj} is constant for these data. After the first injection, $t_{\text{idle}} \leq 8$ s which was insufficient to maintain $P_{\text{CCTBA}}^{\text{HS}} \approx P_{\text{CCTBA}}^{\text{VP}}$. The $m_{\text{inj}}^{\text{m}}$ and $\bar{\eta}_{\text{S}}$ values increase with increasing t_{idle} as more CCTBA diffuses into the head space prior to an injection. The dashed and dot-dashed lines in Fig. 5(d) to 5(f) represent the $m_{\text{inj}}^{\text{c}}$ values calculated with the respective $\bar{\eta}_{\text{S}}$ valves from only the run with t_{idle} = 8 s. This represents the maximum efficiency that can be obtained for these conditions at a stable mass carryover. Overall, the $\bar{\eta}_{\text{S}}$ value at a condition of stable carryover ranges from ≈ 0.23 at shorter t_{idle}, higher $F_{\mathrm{Ar}}^{\mathrm{STP}}$, and lower P^{CDG2} to ≈ 0.71 at longer t_{idle}, lower $F_{\mathrm{Ar}}^{\mathrm{STP}}$, and higher P^{CDG2} for the conditions investigated here.

Bubbler performance can be described well using an analytical expression based upon the bubbler equation with knowledge of $P_{\mathrm{CCTBA}}^{\mathrm{VP}}$ and $P_{\mathrm{ttl}}^{\mathrm{HS}}$, the latter of which can be estimated with two pressure measurements bracketing the precursor vessel. This is not uniformly the case with the flow over vessel. A reasonable estimate of the mass carryover for the first injection is likely possible using Eq. (2) with knowledge of only $P_{\mathrm{CCTBA}}^{\mathrm{VP}}$ and $P_{\mathrm{ttl}}^{\mathrm{HS}}$ in the absence of pressurization effects, but probably only for short t_{inj}. Under the condition of stable mass carryover the $\bar{\eta}_{\mathrm{S}}$ value also is needed to get reasonable results using this equation. Unfortunately, this value is difficult to predict *a priori* and generally is specific to a set of t_{idle}, $F_{\mathrm{Ar}}^{\mathrm{STP}}$, and P^{CDG2}. Hence, only the relationship between mass carryover and t_{inj} could be estimated for a given $\bar{\eta}_{\mathrm{S}}$ value. If such insight into a process is desirable and an NDIR gas analyzer is not available, the $\bar{\eta}_{\mathrm{S}}$ value can be estimated by comparing m_{inj}^{1} to an $m_{\mathrm{inj}}^{\mathrm{m}}$ value obtained by alternative methods such as measuring 1) the overall mass decrease of a precursor vessel or 2) the precursor mass trapped in a cold finger. Either such method would involve a number of injections large enough to make the contribution from the injections prior to a stable output being achieved negligible. An alternative approach to predicting flow over vessel mass carryover is to utilize CFD simulations, although knowledge of the D_{AB} value is necessary for such simulations. Figure 6 shows the $m_{\mathrm{inj}}^{\mathrm{m}}$ values as a function of injection number for the flow over vessel with $F_{\mathrm{Ar}}^{\mathrm{STP}}$ = 0.75 L/min, t_{inj} = 2 s, t_{idle} = 8 s, and in the TV-2 flow configuration. The dot-dashed line represents the corresponding m_{inj}^{1} values. Also shown are the results from two CFD simulations with d_0 = 3.5 × 10^{-5} kg·m·s^{-3}·K$^{-3/2}$ and d_0 = 4.4 × 10^{-4}

kg·m·s^{-3}·K$^{-3/2}$ ($m_{\mathrm{inj}}^{\mathrm{H_2O}}$). The selection of the former d_0 value was described in Sec. 2.5 while the selection of the latter d_0 value was made to approximate the D_{AB} value for water vapor in argon under these conditions. For this latter D_{AB} approximation, reported σ_{AB} = 2.673 Å and Ω_{D} = 535.21 K values for water[39] and σ_{AB} = 3.35 Å and Ω_{D} = 143.2 K values for argon[40] were utilized while all other values were unchanged from the $m_{\mathrm{inj}}^{\mathrm{CFD}}$ simulation. The $m_{\mathrm{inj}}^{\mathrm{m}}$ values correspond to $\bar{\eta}_{\mathrm{S}} = 0.76$ for the first injection and $\bar{\eta}_{\mathrm{S}} = 0.40$ for the fifteenth injection. The $m_{\mathrm{inj}}^{\mathrm{CFD}}$ values are in good agreement after the first three injections. The difference between these masses for the first three injections is attributed to the pressure stabilization process discussed previously (see Figures 2 and 3). For the $m_{\mathrm{inj}}^{\mathrm{CFD}}$ values, $\bar{\eta}_{\mathrm{S}} = 0.96$ for the first injection which is presumably the approximate value expected in the absence of the pressure stabilization process. The CFD simulations can also provide additional insight into the factors affecting mass carryover. For example, a larger diffusion coefficient results in a larger mass carryover since more precursor diffuses into the head space during the idle, as shown by the $m_{\mathrm{inj}}^{\mathrm{H_2O}}$ values in Fig. 6. These values correspond to more than twice the mass carryover at stable output compared to $m_{\mathrm{inj}}^{\mathrm{m}}$ and to $\bar{\eta}_{\mathrm{S}} = 0.97$ and $\bar{\eta}_{\mathrm{S}} = 0.85$ for first and the fifteenth injection, respectively. Although mass carryover increases with increasing diffusion coefficient, the flow over vessel still exhibits a decrease in mass carryover with increasing injection number for a reasonable t_{idle} duration (as reflected by $\bar{\eta}_{\mathrm{S}}$ < unity), even for the unrealistically large diffusion coefficient (for CCTBA) with which $m_{\mathrm{inj}}^{\mathrm{H_2O}}$ was generated. Another obvious way to increase mass carryover is to increase vapor pressure: mass carryover scales directly with vapor pressure (data not shown). However, the $\bar{\eta}_{\mathrm{S}}$ value does not change. In addition, increasing the vapor pressure by increasing the temperature can lead to a greater degree of precursor decomposition. In addition to an $\bar{\eta}_{\mathrm{S}}$ value, validated CFD simulations can also provide $\eta_{\mathrm{S}}(t)$.

Furthermore, unlike $\eta_S(t)$ estimates obtained from measurements external to the vessel, $\eta_S(t)$ values obtained from CFD simulations are unaffected by the presence of any valves or other flow restrictions between the vessel and the measurement location that could distort $\eta_S(t)$.

4. Conclusions

The performance of a bubbler and a flow over vessel were compared for delivery of a low-volatility liquid organometallic precursor for reduced-pressure, cyclical deposition processes. In the case of the bubbler, the mass carryover exhibited little dependence on injection number or t_{idle}, as expected for conditions resulting in the vessel head space being saturated with precursor. Furthermore, the carryover increased with increasing t_{inj}, decreasing P^{CDG2}, and increasing F_{Ar}^{STP}. These relationships were described well using an analytical model based upon the bubbler equation with values for P_{CCTBA}^{VP} and P_{ttl}^{HS}. In the case of the flow over vessel, the mass carryover tended to decrease with injection number until a stable carryover was achieved. Furthermore, the carryover exhibited a dependence on process conditions that varied as this carryover decrease proceeded. For the first injection, the mass carryover was independent of t_{idle} and increased with increasing t_{inj}, decreasing P^{CDG2}, and increasing F_{Ar}^{STP}, as was observed for the bubbler. Once a stable mass carryover was achieved, the mass carryover increased with increasing t_{idle}, increasing t_{inj}, decreasing P^{CDG2}, and decreasing F_{Ar}^{STP}. The change in the dependence of mass carryover on t_{idle} and F_{Ar}^{STP} was attributed to the gas flow dynamics in the flow over vessel. The analytical model could provide a reasonable estimate of the mass carryover for the first injection after a long idle time, although presumably only for short injection times. With knowledge of $\bar{\eta}_S$, the model could describe the flow over vessel performance under the conditions of a stable mass carryover, but only for the dependence of mass carryover on injection time and for a particular combination of

F_{Ar}^{STP}, P^{CDG2}, and t_{idle} corresponding to that $\bar{\eta}_S$ value. CFD simulations described the flow over vessel performance well, after estimating the CCTBA-argon binary diffusion coefficient. These simulations were also used to quantitatively examine the effects on mass carryover of increasing the binary diffusion coefficient and vapor pressure. The results indicate that it is difficult to avoid the initial decrease in mass carryover until a stable mass output is achieved except at long t_{idle}. Hence, it is likely that a vent/run gas manifold configuration would be necessary if a more stable output is needed from a flow over vessel. While these results were obtained with CCTBA, the general relationships between mass carryover and different process parameters in a bubbler and flow over vessel are expected to be similar for other low-volatility precursors. For compounds with higher volatilities than CCTBA, different relationships may be observed than those for low-volatility compounds, depending on the specific precursor properties and vessel design. For example, an increase in volatility without a concomitant increase in diffusivity will result in an increase in the precursor partial pressure without altering the time-dependance of the partial pressure, for both the bubbler and the flow over vessel. In the case of the flow over vessel, therefore, the initial decrease in carryover until a stable carryover is achieved likely would still be observed. However, the magnitude of the initial decrease in carryover would likely be reduced if both volatility and diffusivity increase (for example, see $m_{inj}^{H_2O}$ in Fig. 6). A complicating factor for both vessel designs is that of evaporative cooling. As the vapor pressure increases, the mass carryover increases (all else being constant), and the amount of heat being removed from the system increases. If the heat removed exceeds the heat that can be supplied by the vessel heating system, then the precursor will cool until the heat removed equals the heat supplied. As temperature decreases, vapor pressure and mass carryover will also decrease.

Appendix A. List of symbols.

A_A	Antoine equation constant
ALD	Atomic layer deposition
B_A	Antoine equation constant
CCTBA	μ^2-η^2-(^{t}Bu-acetylene) dicobalthexacarbonyl
CDG1	Upstream capacitance diaphragm gauge
CDG2	Downstream capacitance diaphragm gauge
CFD	Computational fluid dynamics
CVD	Chemical vapor deposition
d_0	Term used in the calculation of the binary diffusion coefficient for CFD simulations
D_{AB}	Binary diffusion coefficient
f_D	Correction term in the calculation of the D_{AB}
FC1	Upstream optical flow cell
FC2	Downstream optical flow cell
F_{Ar}^{STP}	Volumetric flow rate of argon carrier gas at STP
F_{CCTBA}^{STP}	Volumetric flow rate of CCTBA at STP
g	Acceleration of gravity
k_B	Boltzmann constant
l	Length of the dip tube below the CCTBA level in the bubbler
m_A	Molecular mass of molecule A in the calculation of the D_{AB}
m_B	Molecular mass of molecule B in the calculation of the D_{AB}
m_{AB}	Reduced molecular mass of molecules A and B
m_{inj}^{c}	Calculated CCTBA mass delivered per injection from Eq. (2)

$m_{\mathrm{inj}}^{\mathrm{CFD}}$	Simulated CCTBA mass delivered per injection from CFD simulations
$m_{\mathrm{inj}}^{\mathrm{H_2O}}$	Simulated CCTBA mass delivered per injection from CFD simulations using a D_{AB} value corresponding to water vapor in argon.
$m_{\mathrm{inj}}^{\mathrm{m}}$	Measured CCTBA mass delivered per injection
m_{inj}^{1}	Calculated CCTBA mass per injection from Eq. (2) and a perfectly efficient vessel
M	Precursor molar mass
MFC	Mass flow controller
$\mathrm{MV_{in}}$	Manual valve on the saturator inlet line
$\mathrm{MV_{out}}$	Manual valve on the saturator outlet line
n	Number density of molecules
NDIR	Non-dispersive infrared
OMVPE	Organometallic vapor phase epitaxy
P^{CDG1}	Total pressure at CDG1
P^{CDG2}	Total pressure at CDG2
$P_{\mathrm{CCTBA}}^{\mathrm{FC1}}$	CCTBA partial pressure at FC1
$P_{\mathrm{ttl}}^{\mathrm{FC1}}$	Total pressure at FC1
$P_{\mathrm{Ar}}^{\mathrm{HS}}$	Partial pressure of argon carrier gas in the vessel head space
$P_{\mathrm{CCTBA}}^{\mathrm{HS}}$	Partial pressure of CCTBA in the vessel head space
$P_{\mathrm{CCTBA}}^{\mathrm{HS}}(t)$	Time-dependent $P_{\mathrm{CCTBA}}^{\mathrm{HS}}$
$P_{\mathrm{ttl}}^{\mathrm{HS}}$	Total system pressure in the vessel head space
P_{hydro}	Hydrostatic pressure in the bubbler
P^{STP}	Standard pressure

PV_{by}	Pneumatic valve on the saturator bypass line
PV_{in}	Pneumatic valve on the saturator inlet line
PV_{out}	Pneumatic valve on the saturator outlet line
P^{VP}_{CCTBA}	CCTBA vapor pressure
R	Gas constant
STP	Standard temperature and pressure (0 °C and 101.33 kPa)
t_{idle}	duration of the vessel idle between injections
t_{inj}	duration of precursor injection pulse
T	Absolute temperature
T^{STP}	Absolute standard temperature
TV	Throttle valve
TV-1	Designation for the first throttle valve setting employed for measurements
TV-2	Designation for the second throttle valve setting employed for measurements

$\bar{\eta}_S$	Average source efficiency factor
$\eta_S(t)$	Time-dependent instantaneous source efficiency
ρ_{CCTBA}	CCTBA density
σ_{AB}	Characteristic length in the calculation of the D_{AB}
Ω_D	Collision integral in the calculation of the D_{AB}

Declaration of Competing Interest

The authors declare that they have no known competing financial interests or personal relationships that could have appeared to influence the work reported in this paper.

Data availability

Data will be made available on request.

Acknowledgments

The authors gratefully acknowledge B. C. Hendrix (Entegris) for helpful discussions.

References

1. C. L. Andre, N. El-Zein, and N. Tran, Bubbler for constant vapor delivery of a solid chemical, J. Cryst. Growth. 298 (2007) 168-171, https://doi.org/10.1016/j.jcrysgro.2006.10.018
2. R. J. Betsch, Parametric analysis of control parameters in MOCVD, J. Cryst. Growth. 77 (1986) 210-218, https://doi.org/10.1016/0022-0248(86)90303-9
3. B. R. Butler and J. P. Stagg, Variations in Trimethylindium Partial-Pressure Measured by an Ultrasonic Cell on MOVPE Reactor, J. Cryst. Growth. 94 (1989) 481-487, https://doi.org/10.1016/0022-0248(89)90025-0
4. D. M. Frigo, W. W. Vanberkel, W. A. H. Maassen, G. P. M. Vanmier, J. H. Wilkie, and A. W. Gal, A method for dosing solid sources for movpe - excellent reproducibility of dosimetry from a saturated solution of trimethylindium, J. Cryst. Growth. 124 (1992) 99-105, https://doi.org/10.1016/0022-0248(92)90444-n

5. N. D. Gerrard, L. M. Smith, A. C. Jones, and J. Bosnell, An Improved Method of Trimethylindium Transport for the Growth of Indium-Phosphide and Related Alloys by MOVPE, J. Cryst. Growth. 121 (1992) 500-506, https://doi.org/10.1016/0022-0248(92)90161-b
6. R. M. Graham, N. J. Mason, P. J. Walker, D. M. Frigo, and R. W. Gedridge, MOVPE Growth of InSb on GaAs Substrates, J. Cryst. Growth. 124 (1992) 363-370, https://doi.org/10.1016/0022-0248(92)90485-2
7. S. D. Hersee and J. M. Ballingall, The operation of metalorganic bubblers at reduced pressure, J. Vac. Sci. Technol. A. 8 (1990) 800-804, https://doi.org/10.1116/1.576921
8. W. L. Holstein, Performance of gas saturators in the presence of exit stream temperature gradients and implications for chemical vapor deposition saturator design, Chem. Eng. Sci. 49 (1994) 2097-2105,
9. A. Love, S. Middleman, and A. K. Hochberg, The dynamics of bubblers as vapor delivery systems, J. Cryst. Growth. 129 (1993) 119-133, https://doi.org/10.1016/0022-0248(93)90441-x
10. F. Maury, F. D. Duminica, and F. Senocq, Optimization of the vaporization of liquid and solid CVD precursors: Experimental and modeling approaches, Chem. Vap. Deposition. 13 (2007) 638-643, https://doi.org/10.1002/cvde.200706600
11. B. Mayer, C. C. Collins, and M. Walton, Transient analysis of carrier gas saturation in liquid source vapor generators, J. Vac. Sci. Technol. A. 19 (2001) 329-344, https://doi.org/10.1116/1.1322646
12. M. S. Ravetz, R. Odedra, L. M. Smith, S. A. Rushworth, A. B. Leese, G. Williams, and R. Kanjolia. "Transport properties for different bubbler designs", in: 2001 International

Conference on Indium Phosphide and Related Materials, Conference Proceedings. IEEE, 2001. pp. 310-313.

13. M. S. Ravetz, L. M. Smith, S. A. Rushworth, A. B. Leese, R. Kanjolia, J. I. Davies, and R. T. Blunt, Properties of solution TMI as an OMVPE source, J. Electron. Mater. 29 (2000) 156-160, https://doi.org/10.1007/s11664-000-0112-6

14. D. V. Shenai, M. L. Timmons, R. L. DiCarlo, G. K. Lemnah, and R. S. Stennick, Correlation of vapor pressure equation and film properties with trimethylindium purity for the MOVPE grown III-V compounds, J. Cryst. Growth. 248 (2003) 91-98, https://doi.org/10.1016/s0022-0248(02)01854-7

15. D. V. Shenai, M. L. Timmons, R. L. DiCarlo, and C. J. Marsman, Correlation of film properties and reduced impurity concentrations in sources for III/V-MOVPE using high-purity trimethylindium and tertiarybutylphosphine, J. Cryst. Growth. 272 (2004) 603-608, https://doi.org/10.1016/j.jcrysgro.2004.09.006

16. D. V. Shenai-Khatkhate, R. L. DiCarlo, C. J. Marsman, R. F. Polcari, R. A. Ware, and E. Woelk, Stable vapor transportation of solid sources in MOVPE of III-V compound semiconductors, J. Cryst. Growth. 298 (2007) 176-180, https://doi.org/10.1016/j.jcrysgro.2006.10.195

17. D. V. Shenai-Khatkhate, R. L. DiCarlo, and R. A. Ware, Accurate Vapor Pressure Equation for Trimethylindium in OMVPE, J. Cryst. Growth. 310 (2008) 2395-2398, https://doi.org/10.1016/j.jcrysgro.2007.11.196

18. D. V. Shenai-Khatkhate, R. A. Ware, R. L. DiCarlo, R. F. Polcari, C. J. Marsman, E. Woelk, and A. G. Keiter, Exceptionally stable vapor delivery of trimethylindium under intense

OMVPE growth conditions, J. Cryst. Growth. 287 (2006) 679-683, https://doi.org/10.1016/j.jcrysgro.2005.10.095

19. L. M. Smith, R. Odedra, A. Kingsley, K. M. Coward, S. A. Rushworth, G. Williams, T. A. Leese, A. J. Purdie, and R. K. Kanjolia, Trimethylindium transport studies: the effect of different bubbler designs, J. Cryst. Growth. 272 (2004) 37-41, https://doi.org/10.1016/j.jcrysgro.2004.08.108
20. J. P. Stagg, Reagent concentration measurements in metal organic vapour phase epitaxy (MOVPE) using an ultrasonic cell, Chemtronics. 3 (1988) 44-49,
21. J. P. Stagg, J. Christer, E. J. Thrush, and J. Crawley, Measurement and control of reagent concentrations in MOCVD reactor using ultrasonics, J. Cryst. Growth. 120 (1992) 98-102, https://doi.org/10.1016/0022-0248(92)90371-o
22. P. D. Szkutnik, L. Angelides, V. Todorova, and C. Jimenez, Qualification of a sublimation tool applied to the case of metalorganic chemical vapor deposition of In2O3 from In(tmhd)(3) as a solid precursor, Rev. Sci. Instrum. 87 (2016) https://doi.org/10.1063/1.4940930
23. M. Timmons, P. Rangarajan, and R. Stennick, A study of cylinder design for solid OMVPE sources, J. Cryst. Growth. 221 (2000) 635-639, https://doi.org/10.1016/s0022-0248(00)00791-0
24. C. Vahlas, B. Caussat, F. Senocq, W. L. Gladfelter, L. Aloui, and T. Moersch, A delivery system for precursor vapors based on sublimation in a fluidized bed, Chem. Vap. Deposition. 13 (2007) 123-129, https://doi.org/10.1002/cvde.200606513
25. E. Woelk, Performance of a central delivery system for metalorganic precursors, J. Cryst. Growth. 312 (2010) 1340-1342, https://doi.org/10.1016/j.jcrysgro.2009.09.045

26. E. Woelk and R. DiCarlo, Control of vapor feed from liquid precursors to the OMVPE process, J. Cryst. Growth. 393 (2014) 32-34, https://doi.org/10.1016/j.jcrysgro.2013.10.020
27. E. Woelk and R. DiCarlo, Analysis of TMGa output of on-board cylinders for chemical vapor deposition, J. Cryst. Growth. 452 (2016) 226-229, https://doi.org/10.1016/j.jcrysgro.2016.02.036
28. J. E. Maslar, W. A. Kimes, B. A. Sperling, and R. K. Kanjolia, Characterization of bubbler performance for low-volatility liquid precursor delivery, J. Vac. Sci. Technol. A. 37 (2019) https://doi.org/10.1116/1.5099264
29. J. E. Maslar, W. A. Kimes, B. A. Sperling, and R. K. Kanjolia, Characterization of vapor draw vessel performance for low-volatility solid precursor delivery, J. Vac. Sci. Technol. A. 39 (2021) 1-12, https://doi.org/10.1116/6.0000676
30. B. A. Sperling and J. E. Maslar, Experiment-based modeling of a vapor draw ampoule used for low-volatility precursors, J. Vac. Sci. Technol. A. 37 (2019) 060907-060901, https://doi.org/10.1116/1.5125446
31. P. O'Brien, N. L. Pickett, and D. J. Otway, Developments in CVD delivery systems: A chemist's perspective on the chemical and physical interactions between precursors, Chem. Vap. Deposition. 8 (2002) 237-249, https://doi.org/10.1002/1521-3862(20021203)8:6<237::aid-cvde237>3.0.co;2-o
32. C. Vahlas, B. Caussat, W. L. Gladfelter, F. Senocq, and E. J. Gladfelter, Liquid and solid precursor delivery systems in gas phase processes, Recent Pat. Mater. Sci. 8 (2015) 91-108, https://doi.org/DOI: 10.2174/1874464808666150324230711

33. S. Middleman and A. K. Hochberg. "Section 10-4.5. Doping from a Liquid Source - Dynamics of a Bubbler", in: Process Engineering Analysis in Semiconductor Device Fabrication. USA: McGraw-Hill, 1993. pp. 356-360.

34. J. E. Maslar, W. A. Kimes, and B. A. Sperling, Apparatus for characterizing gas-phase chemical precursor delivery for thin film deposition processes, J. Res. Natl. Inst. Stand. Technol. 124 (2019) 124005, https://doi.org/10.6028/jres.124.005

35. J. E. Maslar, W. A. Kimes, B. A. Sperling, and R. K. Kanjolia, Nondispersive infrared gas analyzer for vapor density measurements of a carbonyl-containing organometallic cobalt precursor, Appl. Spectrosc. 71 (2017) 2632-2642, https://doi.org/10.1177/0003702817716939

36. T. Blomberg, Unit steps of an ALD half-cycle, ECS Trans. 58 (2013) 3-18, https://doi.org/10.1149/05810.0003ecst

37. E. W. Lemmon, M. L. Huber, and M. O. McLinden, "NIST Standard Reference Database 23, NIST Reference Fluid Thermodynamic and Transport Properties Database (REFPROP)", Version 9.1 (Gaithersburg, MD, 2013).

38. B. E. Poling, J. M. Prausnitz, and J. P. O'Connell. "11-3 Diffusion coefficients for binary gas systems at low pressures: prediction from theory", in: The Properties of Gases and Liquids. New York, NY: McGraw-Hill, 2001. 11, pp. 11.15-11.19.

39. P. H. Paul, "DRFM: A New Package for the Evaluation of Gas-Phase-Transport Properties", Sandia National Laboratories report SAND98-8203 UC-1409 (1997).

40. R. A. Aziz, A highly accurate interatomic potential for argon, J. Chem. Phys. 99 (1993) 4518-4525, https://doi.org/10.1063/1.466051

Figure captions

Figure 1. A schematic diagram of the flow system for the (a) bubbler and (b) flow over vessel. CDG1 and CDG2, capacitance diaphragm gauges; PV_{in}, PV_{by}, and PV_{out}, pneumatically actuated diaphragm valves; MV_{in} and MV_{out}, manual diaphragm valves; FC1 and FC2, optical flow cells; TV, throttle valve. The drawing is not to scale.

Figure 2. The $m_{\mathrm{inj}}^{\mathrm{m}}$ values as a function of injection number for the bubbler (circles) and flow over vessel (diamonds) with $F_{\mathrm{Ar}}^{\mathrm{STP}}$ = 0.50 L/min, t_{inj} = 2 s, t_{idle} = 8 s, and in the TV-2 flow configuration. The respective $m_{\mathrm{inj}}^{\mathrm{c}}$ values for the bubbler (dashed line) and flow over vessel (dot-dashed lines) were calculated using the $\bar{\eta}_{\mathrm{S}}$ values indicated on each line.

Figure 3. The time-dependent (a) $P_{\mathrm{CCTBA}}^{\mathrm{FC}}$ and (b) P^{CDG2} for the first five injections from the bubbler and (c) $P_{\mathrm{CCTBA}}^{\mathrm{FC}}$ and (d) P^{CDG2} for the first ten injections from the flow over vessel with $F_{\mathrm{Ar}}^{\mathrm{STP}}$ = 0.50°L/min, t_{inj} = 2 s, t_{idle} = 8 s, and in the TV-2 flow configuration.

Figure 4. The $m_{\mathrm{inj}}^{\mathrm{m}}$ value as a function of t_{inj} for the TV-1 and TV-2 flow configurations with the bubbler for $F_{\mathrm{Ar}}^{\mathrm{STP}}$ = (a) 0.25 L/min, (b) 0.50 L/min, and (c) 0.75 L/min and the flow over vessel for $F_{\mathrm{Ar}}^{\mathrm{STP}}$ = (d) 0.25 L/min, (e) 0.50 L/min, and (f) 0.75 L/min. The respective $m_{\mathrm{inj}}^{\mathrm{c}}$ values for the TV-1 configuration (dashed line) and TV-2 configuration (dot-dashed lines) were calculated using the $\bar{\eta}_{\mathrm{S}}$ values indicated on each line. For each injection, $t_{\mathrm{idle}} = 4 \times t_{\mathrm{inj}}$. The data in the bottom panels are offset on the time scale for clarity.

Figure 5. The $m_{\mathrm{inj}}^{\mathrm{m}}$ value as a function of t_{idle} for the TV-1 and TV-2 flow configurations with the bubbler for $F_{\mathrm{Ar}}^{\mathrm{STP}}$ = (a) 0.25 L/min, (b) 0.50 L/min, and (c) 0.75 L/min and the flow over vessel for $F_{\mathrm{Ar}}^{\mathrm{STP}}$ = (d) 0.25 L/min, (e) 0.50 L/min, and (f) 0.75 L/min. The respective $m_{\mathrm{inj}}^{\mathrm{c}}$ values for the TV-1 configuration (dashed line) and TV-2 configuration (dot-dashed lines) were calculated using the $\bar{\eta}_{\mathrm{S}}$ values indicated on each line. For all injections, $t_{\mathrm{inj}} = 0.5$ s. The data in the bottom panels are offset on the time scale for clarity.

Figure 6. The $m_{\mathrm{inj}}^{\mathrm{m}}$ values (circles) and corresponding m_{inj}^{1} values (dot-dashed line) as a function of injection number for the flow over vessel with $F_{\mathrm{Ar}}^{\mathrm{STP}}$ = 0.75 L/min, $t_{\mathrm{inj}} = 2$ s, $t_{\mathrm{idle}} = 8$ s, and in the TV-2 flow configuration. Also shown are the results from two CFD simulations with $d_0 = 3.5 \times 10^{-5}$ kg·m·s^{-3}·K$^{-3/2}$ ($m_{\mathrm{inj}}^{\mathrm{CFD}}$) and $d_0 = 4.4 \times 10^{-4}$ kg·m·s^{-3}·K$^{-3/2}$ ($m_{\mathrm{inj}}^{\mathrm{H_2O}}$).

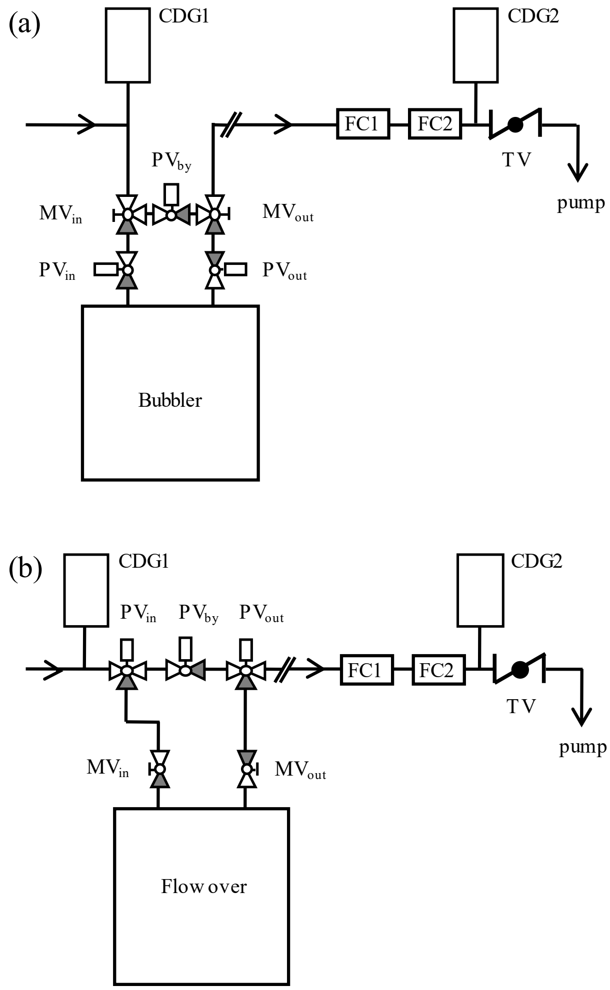
(a)
CDG1
CDG2
FC1
FC2
TV
pump
PV$_{by}$
MV$_{in}$
MV$_{out}$
PV$_{in}$
PV$_{out}$
Bubbler
(b)
CDG1
CDG2
PV$_{in}$
PV$_{by}$
PV$_{out}$
FC1
FC2
TV
pump
MV$_{in}$
MV$_{out}$
Flow over

Figure 1.

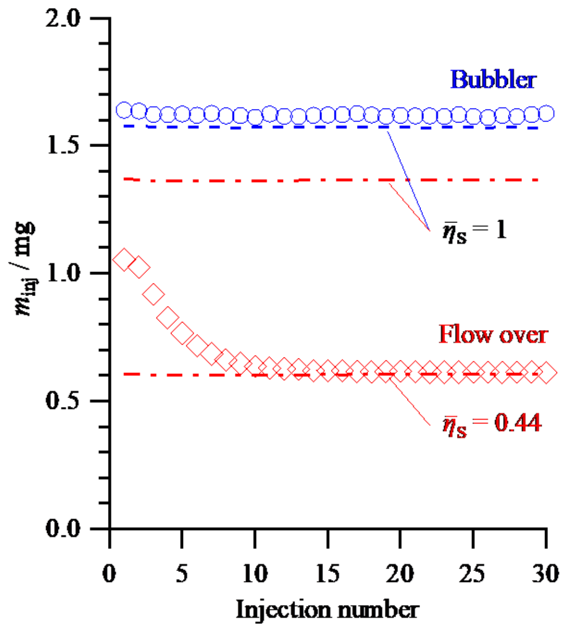
2.0
1.5
1.0
0.5
0.0
m_{inj} / mg
Bubbler
$\bar{\eta}_S = 1$
Flow over
$\bar{\eta}_S = 0.44$
0
5
10
15
20
25
30
Injection number

Figure 2.

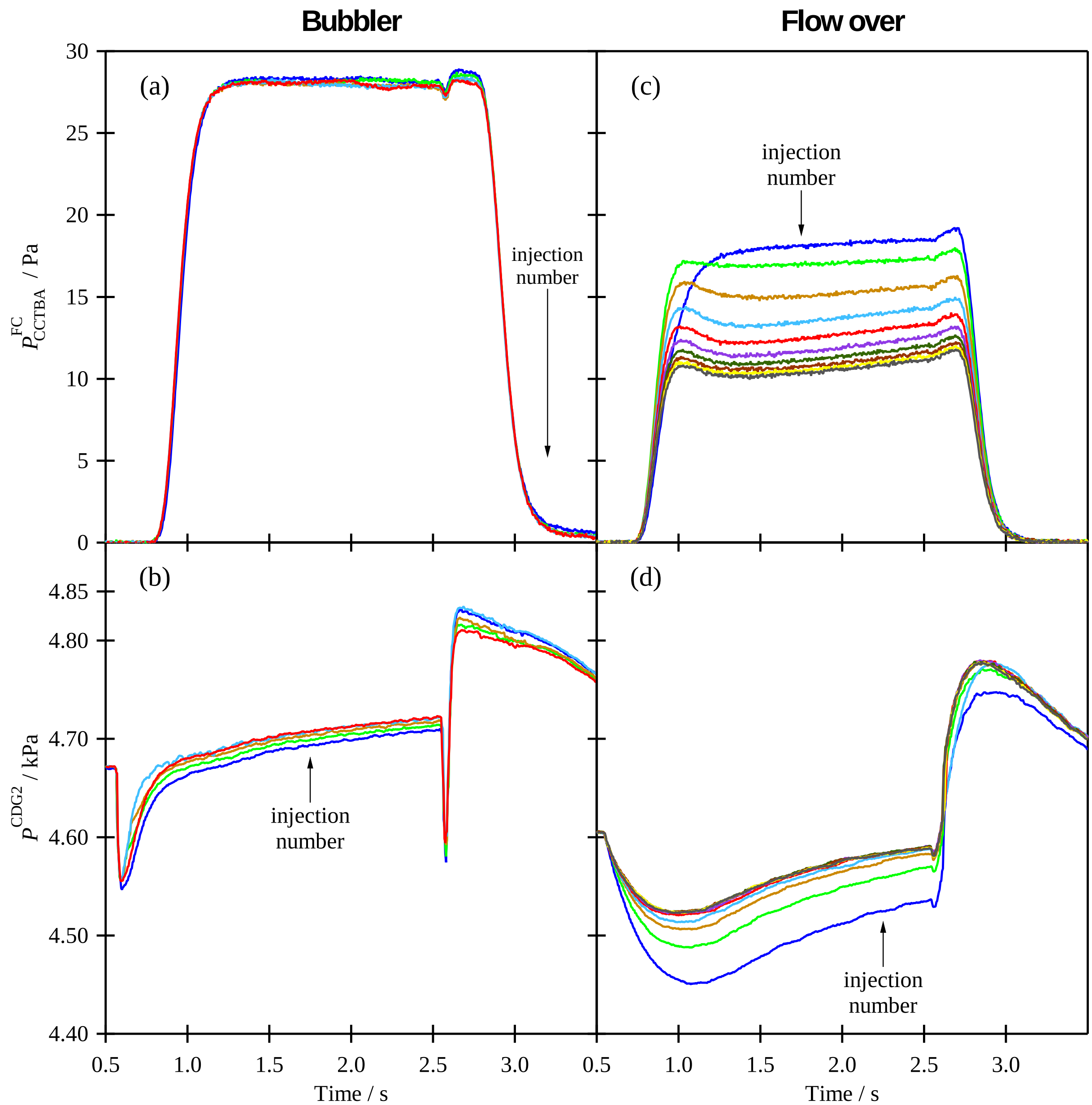

Bubbler
Flow over
(a)
(b)
(c)
(d)
injection number
injection number
injection number
injection number
P^{FC}_{CCTBA} / Pa
P^{CDG2} / kPa
Time / s
Time / s
30
25
20
15
10
5
0
4.85
4.80
4.70
4.60
4.50
4.40
0.5
1.0
1.5
2.0
2.5
3.0

Figure 3.

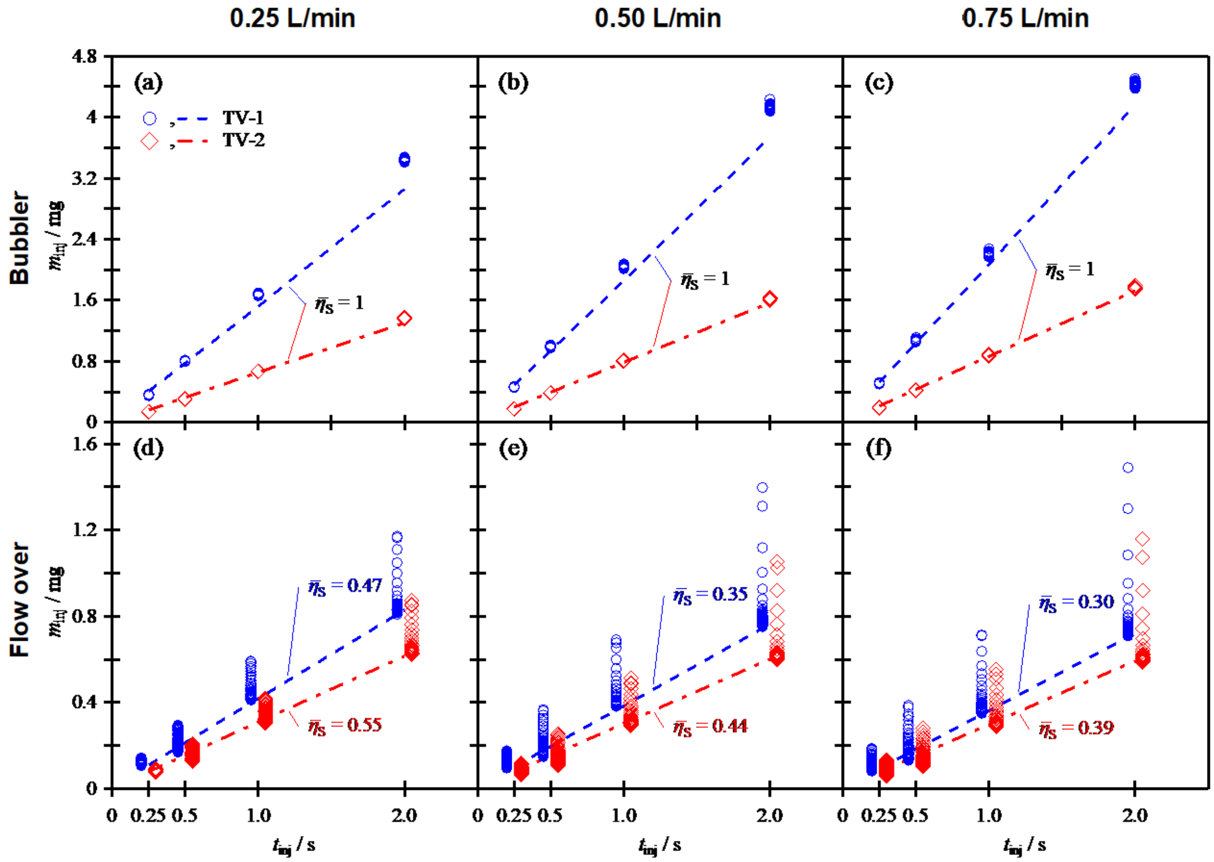
0.25 L/min
0.50 L/min
0.75 L/min
Bubbler
Flow over
(a)
(b)
(c)
(d)
(e)
(f)
TV-1
TV-2
$\bar{\eta}_S = 1$
$\bar{\eta}_S = 0.47$
$\bar{\eta}_S = 0.55$
$\bar{\eta}_S = 0.35$
$\bar{\eta}_S = 0.44$
$\bar{\eta}_S = 0.30$
$\bar{\eta}_S = 0.39$
m_{inj} / mg
t_{inj} / s

Figure 4.

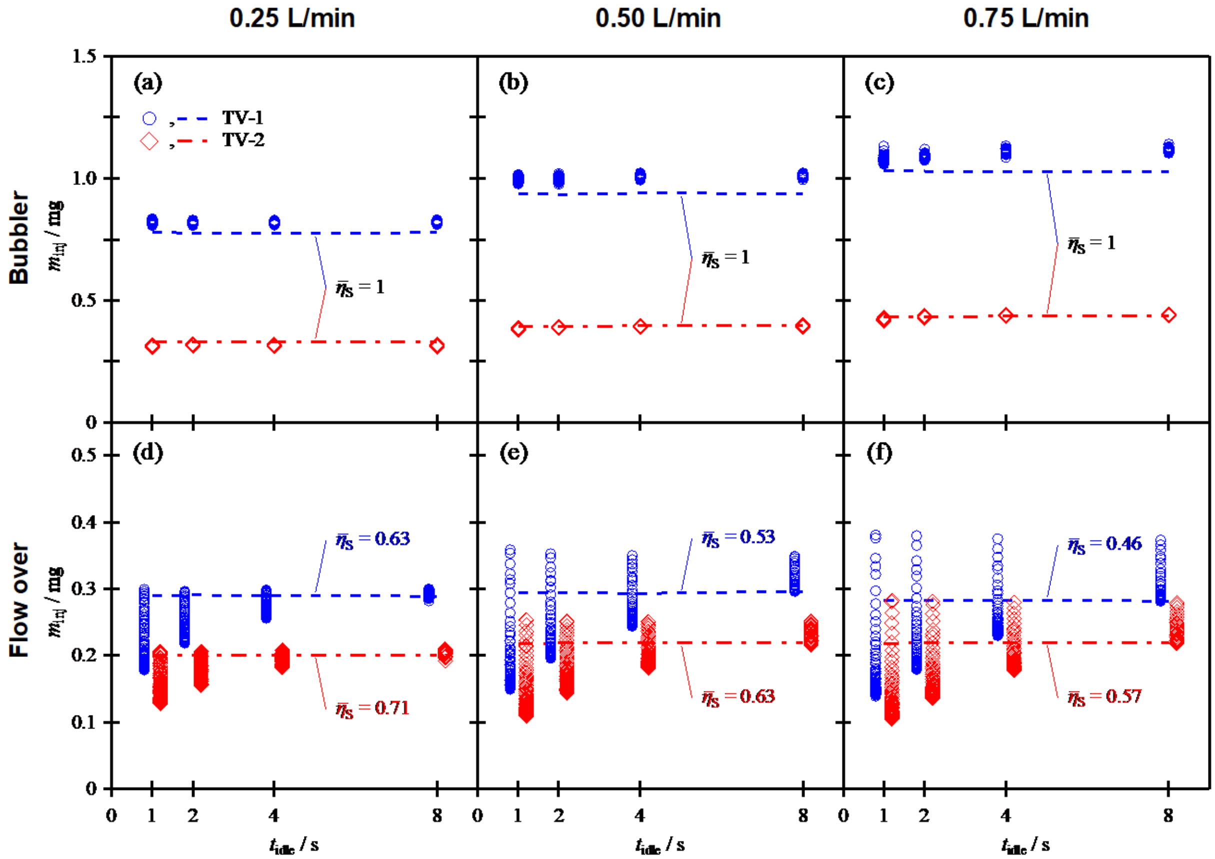
0.25 L/min
0.50 L/min
0.75 L/min
Bubbler
Flow over
(a)
(b)
(c)
(d)
(e)
(f)
TV-1
TV-2
m_{inj} / mg
$\bar{\eta}_S = 1$
$\bar{\eta}_S = 0.63$
$\bar{\eta}_S = 0.71$
$\bar{\eta}_S = 0.53$
$\bar{\eta}_S = 0.63$
$\bar{\eta}_S = 0.46$
$\bar{\eta}_S = 0.57$
t_{idle} / s

Figure 5.

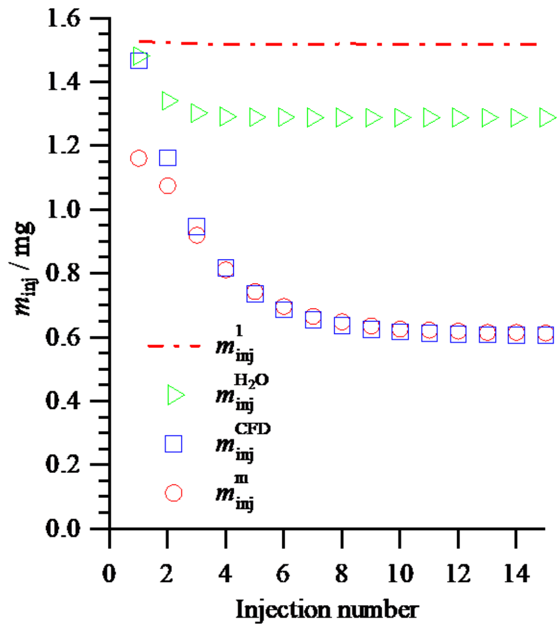

1.6
1.4
1.2
1.0
0.8
0.6
0.4
0.2
0.0
m_{inj} / mg
m_{inj}^{1}
$m_{inj}^{H_2O}$
m_{inj}^{CFD}
m_{inj}^{m}
0
2
4
6
8
10
12
14
Injection number

Figure 6.